
ESTIMATING CONDITION NUMBER WITH GRAPH NEURAL NETWORKS*

PREPRINT

 **Erin Carson**[†]
 Charles University
 Prague, Czech
 carson@karlin.mff.cuni.cz

 **Xinye Chen**
 Sorbonne Université, CNRS, LIP6
 Paris, France
 xinye.chen@lip6.fr

March 17, 2026

ABSTRACT

For large sparse matrices, we almost never compute the condition number exactly because that would require computing the full SVD or full eigenvalue decomposition. In this paper, we propose a fast method for estimating the condition number of sparse matrices using graph neural networks (GNNs). To enable efficient training and inference of GNNs, our proposed feature engineering for GNNs achieves $O(\text{nnz} + n)$, where nnz is the number of non-zero elements in the matrix and n denotes the matrix dimension. We propose two prediction schemes for estimating the matrix condition number using GNNs. One follows by decomposing the condition number and predicts the relatively more computationally intensive part $\|\mathbf{A}^{-1}\|$, while the other is to predict the whole condition number κ . Our approach can be extended to an arbitrary norm. The extensive experiments for the two schemes are conducted for 1-norm and 2-norm condition number estimation, which show that our method achieves a significant speedup over the traditional numerical estimation methods.

Keywords matrix condition number, graph neural networks, AI for numerical methods

1 Introduction

The condition number $\kappa(\mathbf{A})$ of a matrix $\mathbf{A} \in \mathbb{R}^{n \times n}$ quantifies the sensitivity of linear system solutions to perturbations in the input data. For a nonsingular matrix \mathbf{A} , the condition number with respect to the p -norm is defined as:

$$\kappa_p(\mathbf{A}) = \|\mathbf{A}\|_p \cdot \|\mathbf{A}^{-1}\|_p. \quad (1)$$

Computing the exact condition number $\kappa(A)$ is prohibitively expensive for large sparse matrices, since it requires computing the extreme singular values of A . This typically involves one of the following approaches: (i) full singular value decomposition (SVD), which requires $\mathcal{O}(n^3)$ operations for dense matrices; (ii) Matrix inversion also needs $\mathcal{O}(n^3)$ operations. (iii) Iterative methods for estimating eigenvalues, such as power iteration or Lanczos/Arnoldi algorithms, require $\mathcal{O}(k \cdot \text{nnz}(A))$ computational complexity, where $\text{nnz}(A)$ denotes the number of nonzero entries in A and k represents the number of iterations. For decades, the efficient computation of matrix condition numbers has been recognized as essential for assessing the stability of linear systems and least-squares problems, for example in the context of LU factorization with partial pivoting. Early practices ([5, 7]) focused on inexpensive post-factorization estimates that avoid explicit inversion.

For large and sparse matrices, the exact calculation for the condition number is often not practical because computing $\|A^{-1}\|_1$ exactly would require solving many linear systems or forming A^{-1} explicitly. Given the definition $\kappa_1(A) :=$

*This work is in progress and will be submitted soon.

[†]Supported by the Charles University Research Centre program No. UNCE/24/SCI/005 and the European Union (ERC, inEXASCALE, 101075632). Views and opinions expressed are those of the authors only and do not necessarily reflect those of the European Union or the European Research Council. Neither the European Union nor the granting authority can be held responsible for them.

$|A|_1|A^{-1}|_1$, where the matrix norm $|A|_1$ can be computed directly in $\mathcal{O}(\text{nnz}(A))$ time by the maximum of the sums of the absolute values of each column. For matrices that are sufficiently small to be treated using dense linear algebra routines, $|A^{-1}|_1$ is evaluated using dense solvers. For larger matrices, we estimate $|A^{-1}|_1$ using the Hager–Higham iterative algorithm [5, 7], which prevents explicit inversion by solving a sequence of linear equations

$$Ax^{(k)} = b^{(k)}, \quad (2)$$

where the right-hand sides $b^{(k)}$ are chosen adaptively based on the sign pattern of intermediate iterates in order to approximate the vector that maximizes $|A^{-1}b|_1$. A sparse LU factorization of A is computed once and reused for all linear solves.

However, the aforementioned approximate method for condition number estimation mentioned above is limited to the 1-norm case. For the 2-norm condition number, which requires estimating the ratio of the largest to smallest singular values, one often uses iterative methods such as the Lanczos algorithm (or its bidiagonalization variant) to approximate the extreme singular values [4].

We propose a data-driven approach based on neural networks for condition number estimation for sparse systems that: (i) Extracts structural and numerical features of matrix data in $\mathcal{O}(\text{nnz})$ time; (ii) Trains a deep neural network to predict $\log_{10} \kappa(A)$; (iii) Achieves inference time scales insensitive to, or independent of matrix size.

Additionally, a novel graph machine learning approach is used for rapidly estimating the arbitrary-norm condition number of large sparse matrices arising in scientific computing applications. Unlike traditional iterative methods such as the Hager-Higham method [5, 6], our method uses a graph neural network trained on a comprehensive set of matrix-theoretic features to achieve sub-millisecond inference with controllable accuracy. Numerical experiments demonstrate that our approach achieves a significant speedup over classical methods and sparse solvers while maintaining an acceptable relative error.

This is the first work on leveraging graph learning techniques to address condition number estimation. We believe this work can offer unique insights into the application of AI to scientific computing, particularly the numerical computation of matrix properties. We demonstrate the effectiveness of our approach with a simple neural network architecture and challenging condition number estimation tasks.

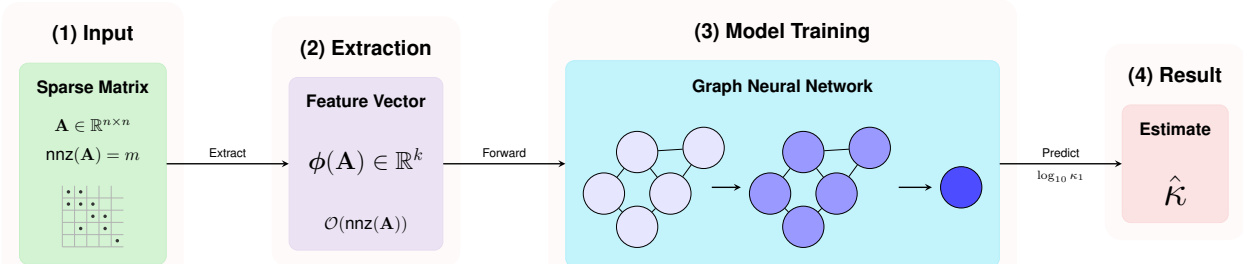


Figure 1: Pipeline for fast condition number estimation. The method consists of four stages: (1) input sparse matrix A , (2) extract matrix-theoretic features, (3) model training using a multilayer perceptron, and (4) output the estimated condition number $\hat{\kappa}(A)$.

The rest of the paper is organized as follows; Section 2 discusses related work on condition number estimation; Section 3 formulates our methodologies, focusing on the matrix features as part of graph construction and model architecture; Section 4 presents our data generation routines for training and analyzes the simulations on performance; Section 5 illustrates the potential shortcomings of our approach, which we leave as future work; Section 6 concludes the paper.

2 Related Work

The foundational contribution in this line of work is due to Cline, Moler, Stewart, and Wilkinson [2], who introduced a simple yet effective estimator based on the solution of two carefully chosen linear systems. Their approach, which was incorporated into the LINPACK library, produces a lower bound on the one-norm condition number at the cost of only a pair of triangular solves. While computationally attractive, the method may underestimate the true condition number by one or more orders of magnitude in certain pathological cases.

A significant improvement appeared shortly thereafter when Hager [5] reformulated the one-norm estimation problem as a convex optimization task. By interpreting $\|A^{-1}\|_1$ as the maximum of $\|A^{-1}x\|_1$ over the unit ball in the one-norm

and deriving an efficient iterative procedure (a specialized variant of the simplex method), Hager’s algorithm typically produces substantially tighter and more reliable estimates than the earlier heuristic, while still requiring only a modest number of matrix–vector products after factorization.

Higham [6] later provided a comprehensive survey of condition-number estimation specifically for triangular matrices—the form that naturally arises after LU factorization. The survey systematically compares growth-factor bounds, residual-based techniques, and inverse-iteration approaches, offering both theoretical insights and practical recommendations regarding the trade-off between accuracy and computational cost. This work serves as a unifying reference and highlights subtle numerical issues that must be addressed when implementing estimators for upper- or lower-triangular factors.

Building directly on Hager’s optimization framework, Higham [7] subsequently proposed a refined one-norm estimator that addresses several practical limitations of the original algorithm. In particular, Higham provided a rigorous convergence analysis, extended the method to complex matrices, introduced safeguards against premature termination, and developed improved stopping criteria that enhance robustness without sacrificing efficiency. These theoretical and algorithmic refinements established a more reliable foundation for condition-number estimation in floating-point arithmetic.

For practical use, Higham [8] later released portable Fortran 77 implementations (subsequently published as Algorithm 674 in [9]). These routines implement the improved one-norm estimator together with its application to condition-number computation, include careful handling of both real and complex arithmetic, and incorporate extensive testing and error-handling mechanisms. The routines were later adopted—with minor modifications—into LAPACK and remain the *de facto* standard in many modern numerical libraries, effectively bridging the gap between theoretical development and robust, widely used software.

Research on predicting condition numbers using machine learning methods remains relatively limited. The only one we realize that has been published is [15], which proposes an approach for predicting the condition number of sparse matrices using support vector regression. Although this method achieves lower accuracy than direct computation or classical estimation techniques, it can still be sufficient for coarse classification tasks, such as determining whether a matrix is well-conditioned or ill-conditioned.

3 Methodology

Consider the supervised learning problem: given a training set $\mathcal{D} = \{(\mathbf{A}_i, \kappa^i)\}_{i=1}^N$ where $\mathbf{A}_i \in \mathbb{R}^{n_i \times n_i}$ are sparse matrices and $\|\cdot\|$ denotes arbitrary norm by removing subscript and same for κ , we seek to construct a rapid estimator by exploiting the factorization

$$\kappa(\mathbf{A}) = \|\mathbf{A}\| \cdot \|\mathbf{A}^{-1}\|. \quad (3)$$

Observing that $\|\mathbf{A}\|$ can be computed exactly in $\mathcal{O}(\text{nnz}(\mathbf{A}))$ time, we reformulate the estimation task: rather than directly predicting $\kappa(\mathbf{A})$, we learn a surrogate function $g : \mathcal{M} \rightarrow \mathbb{R}_+$ such that

$$g(\mathbf{A}) \approx \|\mathbf{A}^{-1}\| \quad \text{or} \quad g(\mathbf{A}) \approx \kappa(\mathbf{A}) \quad \forall \mathbf{A} \in \mathcal{M}, \quad (4)$$

where \mathcal{M} denotes the space of sparse matrices arising in target applications. The condition number estimate is then recovered via the hybrid formula

$$\hat{\kappa}(\mathbf{A}) = \|\mathbf{A}\| \cdot g(\mathbf{A}) \quad \text{or} \quad \hat{\kappa}(\mathbf{A}) = g(\mathbf{A}). \quad (5)$$

Remark 1. *This factorization-based approach offers three key advantages: (i) the learning target $\|\mathbf{A}^{-1}\|$ exhibits smaller dynamic range and improved numerical stability compared to the full condition number; (ii) the exact computation of $\|\mathbf{A}\|$ eliminates one source of approximation error; and (iii) the decomposition aligns with the structure of classical iterative refinement algorithms.*

To stabilize numerical conditioning and improve learning dynamics, we adopt the logarithmic transformation

$$\tilde{g}(\mathbf{A}) = \log_{10} g(\mathbf{A}), \quad (6)$$

So the training target becomes

$$\tilde{\nu}_i = \begin{cases} \log_{10} \|\mathbf{A}_i^{-1}\| = \log_{10} \kappa_i - \log_{10} \|\mathbf{A}_i\|, & \text{if } \hat{\kappa}(\mathbf{A}) = \|\mathbf{A}\| \cdot g(\mathbf{A}) \\ \log_{10} \|\mathbf{A}_i\| \|\mathbf{A}_i^{-1}\|, & \text{if } \hat{\kappa}(\mathbf{A}) = g(\mathbf{A}) \end{cases}$$

and minimize the empirical risk

$$\mathcal{L}(\theta) = \frac{1}{N} \sum_{i=1}^N (\tilde{g}(\mathbf{A}_i; \theta) - \tilde{v}_i)^2, \quad (7)$$

where θ denotes the model parameters. At inference time, the condition number estimate is obtained by exponentiating and combining with the exact norm:

$$\hat{\kappa}(\mathbf{A}) = \|\mathbf{A}\| \cdot 10^{\tilde{g}(\mathbf{A}; \theta^*)} \quad \text{or} \quad \hat{\kappa}(\mathbf{A}) = 10^{\tilde{g}(\mathbf{A}; \theta^*)}, \quad (8)$$

where θ^* are the optimized parameters. In the following, we refer to the two formulas in (8) as the prediction schemes, namely, Scheme 1 and Scheme 2.

3.1 Matrix Features

Direct application of deep learning to matrix inputs faces two fundamental challenges: (i) variable matrix dimensions preclude fixed-size network architectures, and (ii) the computational cost of processing $\mathcal{O}(n^2)$ or $\mathcal{O}(\text{nnz}(\mathbf{A}))$ entries exceeds the cost of traditional methods. We circumvent these obstacles through a carefully designed feature extraction operator $\Phi : \mathbb{R}^{n \times n} \rightarrow \mathbb{R}^d$ that maps matrices to fixed-dimensional feature vectors while preserving essential conditioning information.

We associate each sparse matrix $\mathbf{A} \in \mathbb{R}^{n \times n}$ with a compact d -dimensional feature vector $\phi(\mathbf{A})$ that encodes a rich collection of structural, numerical, and spectral properties known to be predictive of matrix conditioning and the performance of iterative solvers. We write the mapping $\phi : \mathbb{R}^{n \times n} \rightarrow \mathbb{R}^d$, $\mathbf{A} \mapsto \phi(\mathbf{A})$. Following this, we propose a linear complexity algorithm with respect to nnz for feature extraction approach. The vector is formed by concatenating eight complementary groups of descriptors, all computable in $\mathcal{O}(\text{nnz}(\mathbf{A}) + n)$ time:

$$\phi(\mathbf{A}) = \phi_{\text{struc}}(\mathbf{A}) \parallel \phi_{\text{diag}}(\mathbf{A}) \parallel \phi_{\text{norm}}(\mathbf{A}) \parallel \phi_{\text{ddom}}(\mathbf{A}) \parallel \phi_{\text{rsp}}(\mathbf{A}) \parallel \phi_{\text{nzval}}(\mathbf{A}) \parallel \phi_{\text{gers}}(\mathbf{A}) \quad (9)$$

- **Structural descriptors.** These capture the overall scale and sparsity level:

$$\phi_{\text{struc}} = \left(\log_{10}(n + 1), \log_{10}(\text{nnz}(\mathbf{A}) + 1), \frac{\text{nnz}(\mathbf{A})}{n^2} \right)^\top \in \mathbb{R}^3.$$

- **Diagonal properties.** Let $\mathbf{d} = \text{diag}(\mathbf{A})$. We extract statistical moments and range information (in absolute value):

$$\begin{aligned} \phi_{\text{diag}} = & \left(\log_{10}(\mu(|\mathbf{d}|) + \epsilon), \log_{10}(\sigma(|\mathbf{d}|) + \epsilon), \right. \\ & \left. \log_{10}(\min |\mathbf{d}| + \epsilon), \log_{10}(\max |\mathbf{d}| + \epsilon), \right. \\ & \left. \log_{10}\left(\frac{\max |\mathbf{d}|}{\min |\mathbf{d}| + \epsilon}\right) \right)^\top \in \mathbb{R}^5, \end{aligned}$$

where $\mu(\cdot)$ and $\sigma(\cdot)$ are the sample mean and standard deviation, and $\epsilon = 10^{-10}$ guards against underflow.

- **Matrix norms.** Scaled 1-, ∞ -, and Frobenius norms together with their ratio quantify global magnitude and row/column imbalance:

$$\begin{aligned} \phi_{\text{norm}} = & \left(\log_{10}(\|\mathbf{A}\|_1 + \epsilon), \log_{10}(\|\mathbf{A}\|_\infty + \epsilon), \log_{10}(\|\mathbf{A}\|_F + \epsilon), \right. \\ & \left. \log_{10}\left(\frac{\|\mathbf{A}\|_1}{\|\mathbf{A}\|_\infty + \epsilon}\right) \right)^\top \in \mathbb{R}^4, \end{aligned}$$

with the standard definitions $\|\mathbf{A}\|_1 = \max_j \sum_i |a_{ij}|$, $\|\mathbf{A}\|_\infty = \max_i \sum_j |a_{ij}|$, and $\|\mathbf{A}\|_F = \sqrt{\sum_{i,j} a_{ij}^2}$. Notably, $\|\mathbf{A}\|_1$ serves dual roles: as a feature for learning and as the exact multiplicative factor in (5).

- **Diagonal-dominance measures.** Motivated by classical convergence criteria for stationary iterative methods, we compute the row-wise dominance ratio

$$\alpha_{\text{row}} = \frac{|\mathbf{d}|}{|\mathbf{r}| + \epsilon \mathbf{1}},$$

where $\mathbf{r} = |\mathbf{A}| \mathbf{1}$ is the absolute row-sum vector. We collect its statistical summary:

$$\phi_{\text{ddom}} = \left(\mu(\alpha_{\text{row}}), \min \alpha_{\text{row}}, \max \alpha_{\text{row}}, \sigma(\alpha_{\text{row}}) \right)^\top \in \mathbb{R}^4.$$

- **Row-sparsity pattern descriptors.** Let $\rho_i = \text{nnz}(\mathbf{A}_{i,:})$ be the number of nonzeros in row i . We summarize the distribution of $\boldsymbol{\rho}$ via logarithmic moments, extrema, and relative dispersion:

$$\begin{aligned} \phi_{\text{rsp}} &= (\log_{10}(\mu(\boldsymbol{\rho}) + 1), \log_{10}(\sigma(\boldsymbol{\rho}) + 1), \log_{10}(\max \boldsymbol{\rho} + 1), \\ &\log_{10}(\min_{\rho_i > 0} \rho_i + 1), \frac{\sigma(\boldsymbol{\rho})}{\mu(\boldsymbol{\rho}) + 1})^\top \in \mathbb{R}^5. \end{aligned}$$

- **Nonzero-value statistics.** Let $\mathcal{S} = \{a_{ij} : a_{ij} \neq 0\}$. Analogous moment and range descriptors on $|\mathcal{S}|$ are

$$\begin{aligned} \phi_{\text{nzval}} &= (\log_{10}(\mu(|\mathcal{S}|) + \epsilon), \log_{10}(\sigma(|\mathcal{S}|) + \epsilon), \\ &\log_{10}(\min |\mathcal{S}| + \epsilon), \log_{10}(\max |\mathcal{S}| + \epsilon), \\ &\log_{10}(\frac{\max |\mathcal{S}|}{\min |\mathcal{S}| + \epsilon}))^\top \in \mathbb{R}^5. \end{aligned}$$

- **Gershgorin-based estimates.** Define the Gershgorin radii $g_i = \sum_{j \neq i} |a_{ij}|$. We retain their logarithmic mean, maximum, and normalized mean:

$$\phi_{\text{gers}} = (\log_{10}(\mu(\mathbf{g}) + \epsilon), \log_{10}(\max \mathbf{g} + \epsilon), \mu(\frac{\mathbf{g}}{|\mathbf{d}| + \epsilon \mathbf{1}}))^\top \in \mathbb{R}^3.$$

Assembling $\phi(\mathbf{A})$ as in (9) requires only $\mathcal{O}(\text{nnz}(\mathbf{A}) + n)$ arithmetic operations, making feature extraction negligible compared with any subsequent condition-number estimation procedure.

3.2 Graph Neural Network Architecture

To leverage the structural information encoded in the sparsity pattern of \mathbf{A} , we represent each matrix as an attributed graph $\mathcal{G} = (\mathcal{V}, \mathcal{E}, \mathbf{X}, \mathbf{E}, \phi)$ where:

- $\mathcal{V} = \{1, \dots, n\}$ is the set of nodes corresponding to matrix rows/columns;
- $\mathcal{E} = \{(i, j) : a_{ij} \neq 0\}$ is the edge set defined by the nonzero pattern;
- $\mathbf{X} \in \mathbb{R}^{n \times 2}$ is the node feature matrix with rows

$$\mathbf{x}_i = (\log_{10}(|a_{ii}| + \epsilon), \log_{10}(\rho_i + 1))^\top, \quad (10)$$

where $\rho_i = \text{nnz}(\mathbf{A}_{i,:})$ is the row sparsity;

- $\mathbf{E} \in \mathbb{R}^{|\mathcal{E}| \times 1}$ is the edge feature matrix with entries

$$e_{ij} = \log_{10}(|a_{ij}| + \epsilon); \quad (11)$$

- $\phi(\mathbf{A}) \in \mathbb{R}^d$ is the global feature vector defined in (9).

Additionally, for the prediction of 1-norm (incl. 2-norm) condition number, we store the exact 1-norm $\|\mathbf{A}\|_1$ (incl. 2-norm) as graph-level metadata for the Scheme 1 in the inference formula (8).

3.2.1 Message Passing Layers

We employ a graph convolutional network (GCN) [11] with K layers to learn node embeddings that capture both local connectivity and nonzero value distributions. The forward pass is specified by:

$$\mathbf{h}_i^{(0)} = \sigma(\mathbf{W}_{\text{node}} \mathbf{x}_i), \quad (12)$$

$$\mathbf{h}_i^{(k+1)} = \sigma \left(\mathbf{W}^{(k)} \sum_{j \in \mathcal{N}(i)} \frac{\mathbf{h}_j^{(k)}}{\sqrt{|\mathcal{N}(i)| |\mathcal{N}(j)|}} \right), \quad k = 0, \dots, K-1, \quad (13)$$

where $\mathcal{N}(i) = \{j : (i, j) \in \mathcal{E}\}$ is the neighborhood of node i , $\mathbf{W}_{\text{node}} \in \mathbb{R}^{\ell \times 2}$ and $\mathbf{W}^{(k)} \in \mathbb{R}^{\ell \times \ell}$ are learnable weight matrices, $\sigma(\cdot)$ denotes the ReLU activation, and ℓ is the hidden dimension.

3.2.2 Graph-Level Aggregation and Prediction

The node embeddings $\{\mathbf{h}_i^{(K)}\}_{i=1}^n$ are aggregated into a graph-level representation via mean and max pooling:

$$\mathbf{z}_{\text{mean}} = \frac{1}{n} \sum_{i=1}^n \mathbf{h}_i^{(K)}, \quad \mathbf{z}_{\text{max}} = \max_{i=1}^n \mathbf{h}_i^{(K)}, \quad (14)$$

where the maximum is taken element-wise. In parallel, the global feature vector $\phi(\mathbf{A})$ is encoded through a separate branch:

$$\mathbf{u} = \sigma(\mathbf{W}_{\text{global}}\phi(\mathbf{A}) + \mathbf{b}_{\text{global}}), \quad (15)$$

with $\mathbf{W}_{\text{global}} \in \mathbb{R}^{\ell \times d}$. The concatenated representation $[\mathbf{z}_{\text{mean}}; \mathbf{z}_{\text{max}}; \mathbf{u}] \in \mathbb{R}^{3\ell}$ is then processed by a prediction head:

$$\begin{aligned} \mathbf{h}^{(0)} &= [\mathbf{z}_{\text{mean}}; \mathbf{z}_{\text{max}}; \mathbf{u}], \\ \mathbf{h}^{(k)} &= \sigma\left(\text{Drop}_q(\mathbf{W}_{\text{out}}^{(k)}\mathbf{h}^{(k-1)} + \mathbf{b}_{\text{out}}^{(k)})\right), \quad k = 1, 2, \dots, L-1, \\ \tilde{g}(\mathbf{A}; \theta) &= \mathbf{W}_{\text{out}}^{(L)}\mathbf{h}^{(L-1)} + \mathbf{b}_{\text{out}}^{(L)}. \end{aligned} \quad (16)$$

where Drop_q denotes dropout with rate q . The complete architecture contains approximately 150,000 trainable parameters. The final condition number estimate is recovered via the hybrid formula (8):

$$\hat{\kappa}_p(\mathbf{A}) = \|\mathbf{A}\|_p \cdot 10^{\tilde{g}(\mathbf{A}; \theta^*)}. \quad (17)$$

The two-stream architecture brings together local graph structure using GCN and global statistical features using MLP. This helps the model learn both detailed sparsity patterns and broader matrix properties. By using $\|\mathbf{A}\|_1$ directly in (17), the neural network can focus on learning the more difficult inverse norm $\|\mathbf{A}^{-1}\|_1$.

4 Numerical Experiments

We evaluate the performance of our method against standard approaches for condition number estimation. Unless otherwise noted, all methods are implemented in PyTorch. Experiments and timing measurements were performed on a server equipped with 1 TB of RAM, dual Intel Xeon Gold 6330 processors (56 cores and 112 threads per processor, 2.00 GHz base frequency), and four NVIDIA A100 GPUs (80 GB PCIe each). All computations were executed on the GPUs.

There are no standard solutions for evaluating condition number for sparse matrices in GPU, particularly in Python environment. The direct call for calculating condition number in Pytorch, there is well-established one called `torch.linalg.cond`; In PyTorch, `torch.linalg.cond` currently does not automatically apply sparse optimizations for sparse matrices. Besides, PyTorch currently does not have sparse LU decomposition. Its internal implementation is based on dense matrices, using SVD (singular value decomposition) or 2-norm/ ∞ -norm computations.

To ensure a comprehensive and fair evaluation, we consider several implementations of the competing approaches. For the computation of the 1-norm condition number, we consider the following methods: ① computing the exact value using `torch.linalg.cond` on GPU; ② using `scipy.sparse.linalg.norm` to compute the matrix 1-norm, `scipy.sparse.linalg.splu` to perform linear solves required for matrix inversion, and `scipy.sparse.linalg.onenormest`³ to estimate the 1-norm of the matrix inverse; ③ applying the Hager–Higham algorithm with `torch.linalg.lu_factor` for LU solves, while keeping the remaining operations implemented in PyTorch on GPU. For the computation of the 2-norm condition number, we consider two approaches: ④ computing the exact value using `torch.linalg.cond` on GPU; ⑤ a GPU-based Golub–Kahan method, i.e., a condition number estimate based on Ritz singular values computed via Golub–Kahan bidiagonalization. Methods ① and ④ are referred to as the exact approaches. Methods ② and ③ are referred to as Hager–Higham (SciPy) and Hager–Higham, respectively. Our proposed approach is referred to as GNN in the following. Our Golub–Kahan method takes the Golub–Kahan Lanczos bidiagonalization for estimating the 2-norm condition number of a matrix. To enhance numerical stability, full reorthogonalization is applied during the iterations using the Modified Gram–Schmidt procedure. Sparse matrices are stored as PyTorch sparse tensors to enable GPU-accelerated computations.

³A Block Algorithm for Matrix 1-Norm Estimation, note that it is to compute a lower bound of the 1-norm of a sparse array (matrix).

4.1 Training Data

To ensure the trained model generalizes across diverse sparse linear systems, we construct a heterogeneous training corpus consisting of matrices from five representative problem classes as follows.

We limit the variation in our training sizes to increments of 1000 (e.g., from 1000 to 2000 or from 3000 to 4000), because increasing the gap would necessarily require more data. However, in this paper, we focus on model performance when trained with a limited amount of data across different machine or GPU scales.

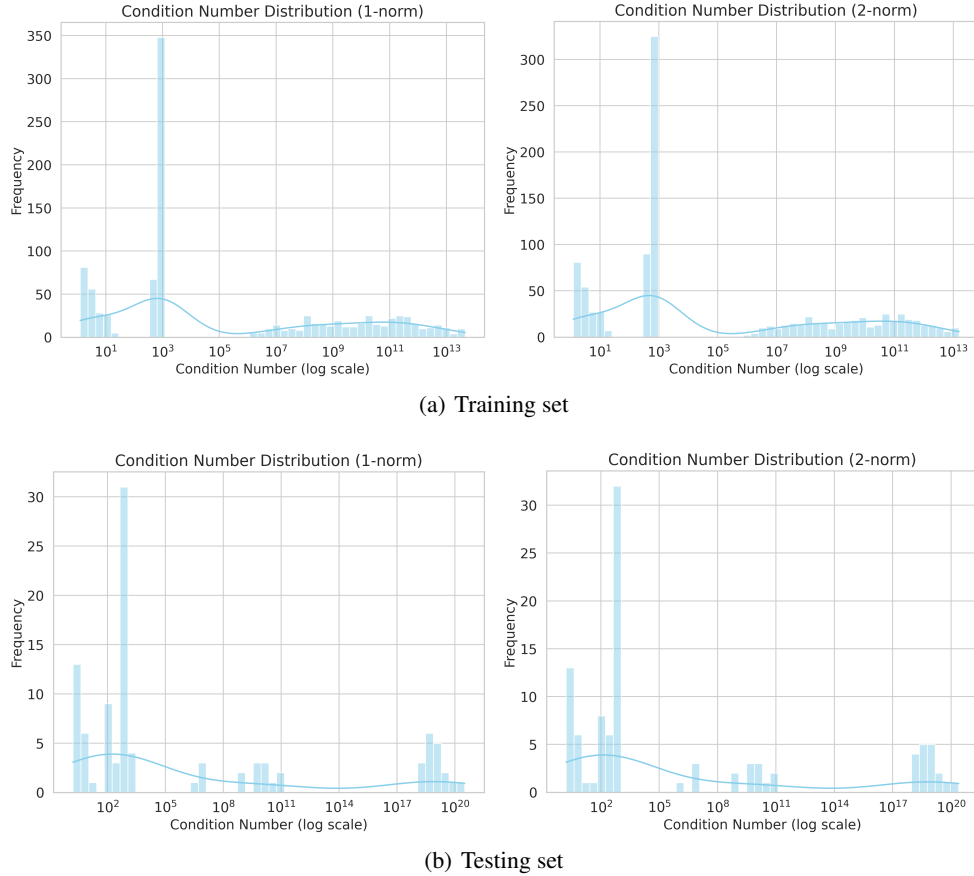


Figure 2: Matrix condition number distribution.

- **Partial Differential Equation Discretizations:**

- **2D Poisson Equation.** The canonical 2D Poisson equation $-\Delta u = f$ on the unit square with homogeneous Dirichlet boundary conditions is discretized on an $m \times m$ uniform grid using the standard 5-point finite difference stencil. This yields the sparse symmetric positive definite matrix $\mathbf{A} \in \mathbb{R}^{n \times n}$ ($n = m^2$) whose nonzero entries satisfy

$$a_{ij} = \begin{cases} 4, & i = j, \\ -1, & |i - j| = 1 \text{ or } |i - j| = m, \\ 0, & \text{otherwise,} \end{cases} \quad (18)$$

with boundary rows and columns modified to enforce the Dirichlet conditions. The matrix has condition number $\kappa_2(\mathbf{A}) = \Theta(m^2) = \mathcal{O}(h^{-2})$ [14].

- **Anisotropic Diffusion Equation.** We further consider the anisotropic diffusion problem

$$-\nabla \cdot (K \nabla u) = f, \quad K = \text{diag}(\varepsilon, 1),$$

with strong anisotropy induced by $\varepsilon \ll 1$. Using the same 5-point stencil on an $m \times m$ grid, the resulting matrix remains symmetric positive definite but becomes highly ill-conditioned for small ε . In our dataset, ε is sampled from the log-uniform distribution $10^{\mathcal{U}(-8, -2)}$.

- High-Contrast Diffusion Problems. Extremely ill-conditioned test cases are generated from the variable-coefficient elliptic equation

$$-\nabla \cdot (\kappa(x, y) \nabla u) = f,$$

where the diffusion coefficient $\kappa(x, y)$ exhibits high contrast. At each grid point we sample $\kappa_i \in [1, 10^c]$ with $c \sim \mathcal{U}(6, 13)$. The matrix is constructed as $\mathbf{A} = \mathbf{S}\mathbf{A}_0\mathbf{S}$, where \mathbf{A}_0 is the standard Poisson matrix (18) and $\mathbf{S} = \text{diag}(\sqrt{\kappa})$. This construction routinely yields condition numbers exceeding 10^{10} , representative of challenging problems in heterogeneous media.

- **Synthetic Random Matrices:**

- Random Ill-Conditioned SPD Matrices. Additional random sparse SPD matrices with explicitly controlled condition numbers are generated as follows:

1. Sample a random sparse matrix $\mathbf{B} \in \mathbb{R}^{n \times n}$ with density 0.1 and entries drawn uniformly from $[0, 1]$.
2. Symmetrize: $\mathbf{C} = (\mathbf{B} + \mathbf{B}^\top)/2$.
3. Enforce strict diagonal dominance:

$$\mathbf{D} = \mathbf{C} + \text{diag}(\mathbf{r} \cdot 1.5 + \mathbf{1}),$$

where \mathbf{r} is the vector of maximum absolute row sums of \mathbf{C} .

4. Control the target condition number $\kappa_{\text{target}} = 10^\tau$ with $\tau \sim \mathcal{U}(7, 13)$. Form the diagonal scaling matrix $\mathbf{S} = \text{diag}(s_i)$, where the s_i are logarithmically spaced values in $[1, \sqrt{\kappa_{\text{target}}}]$ randomly permuted, and set

$$\mathbf{A} = \mathbf{S}\mathbf{D}\mathbf{S}.$$

The resulting matrices span well-conditioned to extremely ill-conditioned regimes (condition numbers up to 10^{13}).

- Symmetric Tridiagonal Matrices. We also include symmetric tridiagonal matrices

$$\mathbf{A} = \text{tridiag}(-\alpha, 2, -\alpha) \in \mathbb{R}^{n \times n},$$

where $\alpha \sim \mathcal{U}(0.1, 0.9)$. These matrices are strictly diagonally dominant (hence positive definite) and possess analytically known eigenvalues

$$\lambda_k = 2 - 2\alpha \cos\left(\frac{k\pi}{n+1}\right), \quad k = 1, \dots, n,$$

facilitating direct validation of learned spectral estimators.

- **2D Convection–Diffusion Equation.** We consider the two-dimensional steady-state convection–diffusion problem

$$-\varepsilon \nabla^2 u + \boldsymbol{\beta} \cdot \nabla u = f, \quad \boldsymbol{\beta} = (\beta_x, \beta_y), \quad (19)$$

on the unit square with homogeneous Dirichlet boundary conditions. Discretization is performed on an $m \times m$ uniform grid ($m = \lceil \sqrt{n} \rceil$) using a standard 5-point finite difference stencil for the diffusion term and an upwind scheme for the convection term.

The resulting linear system is represented by a sparse matrix $\mathbf{A} \in \mathbb{R}^{n \times n}$, $n = m^2$, with entries given by

$$a_{ij} = \begin{cases} 4\varepsilon/h^2 + \text{convection contributions}, & i = j, \\ -\varepsilon/h^2 \pm \text{upwind correction}, & j \in \text{neighbors of } i, \\ 0, & \text{otherwise,} \end{cases}$$

where $h = 1/(m+1)$ denotes the grid spacing and the sign of the upwind correction depends on the flow direction.

Due to the upwind discretization, the matrix \mathbf{A} is generally *nonsymmetric* whenever $\boldsymbol{\beta} \neq \mathbf{0}$, while remaining sparse with at most five nonzero entries per row. The upwind scheme ensures numerical stability for convection-dominated regimes, but explicitly breaks symmetry, distinguishing these matrices from standard symmetric diffusion operators.

The matrices for training, validation, and testing are sampled with equal probability from each class. The generation routines ensure that the matrices used for training and testing exhibit a wide range of condition numbers. The condition numbers for the training and testing set are shown in Figure 2. The statistical information of the generated matrices for training, validation, and testing is shown in Table 1.

Table 1: Statistics of the matrix datasets. Condition numbers are reported with respect to the 1-norm (κ_1) and 2-norm (κ_2). Sparsity is independent of the norm.

Split	# Matrices	Condition number (κ_1)		Condition number (κ_2)		Sparsity mean (range)
		Min	Max	Min	Max	
Train	1000	1.24	8.71×10^{20}	1.24	7.10×10^{20}	96.49% (80.89%–99.85%)
Test	100	1.64	3.21×10^{20}	1.64	2.41×10^{20}	96.88% (80.92%–99.85%)
Validation	100	1.75	1.16×10^{20}	1.75	9.66×10^{19}	96.51% (80.91%–99.84%)

4.2 Training Protocols

We minimize the loss function (7) augmented with L^2 regularization:

$$\mathcal{L}_{\text{reg}}(\theta) = \mathcal{L}(\theta) + \lambda \sum_L \|\mathbf{W}^{(L)}\|_F^2,$$

with regularization parameter $\lambda = 10^{-5}$. We use the Adam algorithm optimizer [10] with learning rate $\alpha = 10^{-3}$ and default momentum parameters $\beta_1 = 0.9$, $\beta_2 = 0.999$. Training proceeds for up to 100 epochs with mini-batch size 32, employing early stopping with patience 20 based on validation set performance.

The learning rate is adaptively reduced by a factor of 0.5 when validation loss plateaus for 10 consecutive epochs, implementing the ReduceLROnPlateau schedule [12]. Gradient clipping with threshold $\tau = 1.0$ is applied to prevent exploding gradients during training. Dropout regularization [13] with a rate of 0.1 is applied after the first two hidden layers of the prediction head to mitigate overfitting prone to model training.

To verify the efficiency of our models and without loss of generality, we restrict the matrix sizes between 1,000 and 2,000, which is medium scale problem. our final training corpus consists of $N_{\text{train}} = 1,000$ matrices with dimensions ranging from 1,000 to 2,000, validation set $N_{\text{val}} = 100$ with the same size range, and test set $N_{\text{test}} = 100$ with dimensions 1,000 to 2,000.

4.3 Evaluation Metrics

For the reference result on the exact value of the condition number, we use the function `torch.linalg.cond` to compute the condition number $\kappa_p(A) = \|A\|_p \cdot \|A^{-1}\|_p$ depending on the chosen norm. When $p = 2$ (i.e., 2-norm), the library employs singular value decomposition to factorize A , and defines the 2-norm condition number as the ratio of the largest to the smallest singular value, i.e., $\kappa_2(A) = \sigma_{\max}/\sigma_{\min}$. This approach delivers high computational stability and is thus the default and most commonly used method. The underlying computations rely on LAPACK routines for numerical linear algebra. For other norms p , it requires explicitly computing the inverse of A and thus is generally less numerically stable than the 2-norm computation based on SVD.

We assess both accuracy and computational efficiency using the following metrics:

- For each test matrix \mathbf{A} , let $\kappa_1(\mathbf{A})$ denote the ground truth condition number and $\hat{\kappa}_1(\mathbf{A})$ the estimate produced by a given method. We define *Logarithmic relative error*:

$$\text{LRE}(\mathbf{A}) = \frac{|\log_{10} \hat{\kappa}_1(\mathbf{A}) - \log_{10} \kappa_1(\mathbf{A})|}{|\log_{10} \kappa_1(\mathbf{A})|}. \quad (20)$$

This normalized variant accounts for the magnitude of the true condition number, with values reported as percentages. In practice, for zero-division protection, a small number is added, e.g. 10^{16} , to the denominator. We aggregate these metrics across the test set via their mean and maximum:

$$\overline{\text{LRE}} = \frac{1}{N_{\text{test}}} \sum_{i=1}^{N_{\text{test}}} \text{LRE}(\mathbf{A}_i), \quad \text{LRE}_{\max} = \max_{1 \leq i \leq N_{\text{test}}} \text{LRE}(\mathbf{A}_i). \quad (21)$$

Unlike standard relative error in linear space, the logarithmic metrics (21) is well-suited to condition numbers spanning multiple orders of magnitude. For instance, a linear relative error of 100% for $\kappa_1 = 10^6$ ($\hat{\kappa}_1 = 2 \times 10^6$) translates to $\text{LRE} \approx 30\%$, correctly reflecting that the estimate remains within the same order of magnitude.

- To evaluate computational efficiency, we measure wall-clock time for each method over $R = 4$ independent runs per test matrix, reporting:

1. **Mean inference time:**

$$T_\mu(\mathbf{A}) = \text{mean} \{t_1(\mathbf{A}), \dots, t_R(\mathbf{A})\}, \quad (22)$$

where $t_r(\mathbf{A})$ is the time for the r -th run. The median is preferred over the mean to mitigate outliers from system-level noise. For task 1), the runtime for GNN also additionally includes the trivial computation of $\|\mathbf{A}\|_1$.

2. **Speedup factor:**

$$S_{\mathcal{M}_1 \rightarrow \mathcal{M}_2}(\mathbf{A}) = \frac{T_\mu^{\mathcal{M}_1}(\mathbf{A})}{T_\mu^{\mathcal{M}_2}(\mathbf{A})}, \quad (23)$$

quantifying how many times faster method \mathcal{M}_2 is compared to exact method \mathcal{M}_1 (performed by `numpy.linalg.cond(A)`). We primarily report $S_{\text{Exact} \rightarrow \text{GNN}}$ and $S_{\text{Higham} \rightarrow \text{GNN}}$.

For the GNN, we decompose the total time as

$$T_{\text{GNN}}(\mathbf{A}) = \begin{cases} T_{\text{feature}}(\mathbf{A}) + T_{\text{inference}}(\mathbf{A}) + T_{\text{norm}}(\mathbf{A}), & \text{if } \hat{\kappa}(\mathbf{A}) = \|\mathbf{A}\| \cdot g(\mathbf{A}), \\ T_{\text{feature}}(\mathbf{A}) + T_{\text{inference}}(\mathbf{A}), & \text{if } \hat{\kappa}(\mathbf{A}) = g(\mathbf{A}). \end{cases}$$

where T_{feature} is the time to construct the graph and extract features $\phi(\mathbf{A})$, $T_{\text{inference}}$ is the forward pass through the GNN, and T_{norm} is the overhead of computing $\|\mathbf{A}\|_1$ and applying (17).

4.4 Empirical Results

Following the above formulation, we focus on the two methodologies on prediction of (1) $g(\mathbf{A}) \approx \|\mathbf{A}^{-1}\|_1$ and (2) $g(\mathbf{A}) \approx \kappa(\mathbf{A})$, $\forall \mathbf{A} \in \mathcal{M}$, respectively. To mitigate the effects of environmental variability, we independently reran all competing methods for each scheme. Due to rounding errors and random initialization, the runtime of the competing methods (e.g., the runtime of the Golub–Kahan method) may vary slightly. This can be observed in the Tables 2 and 3.

Figure 4 in Appendix illustrates the training and validation loss described by mean squared error during training; the error curves for training and validation show almost identical behavior. This training trajectory suggests strong generalization performance and minimal overfitting.

For Scheme 1, where $\hat{\kappa}(\mathbf{A}) = |\mathbf{A}| \cdot 10^{\tilde{g}(\mathbf{A}; \theta)}$, the learning task becomes $\tilde{g}(\mathbf{A}; \theta) \approx \log_{10} |\mathbf{A}^{-1}|$. The runtime and accuracy of the competing methods are reported in Table 2. For both the 1-norm and 2-norm condition numbers, the GNN approach consistently outperforms the Hager–Higham methods and the exact approach in terms of the average runtime. The speedup of GNN over Hager–Higham approach is close to 9–11 \times . For the 1-norm condition number, GNN achieves lower $\overline{\text{LRE}}$ and LRE_{max} than the Hager–Higham method by an order of magnitude. For the 2-norm condition number, GNN is approximately 5–10 \times faster than the Golub–Kahan method, while also achieving substantially smaller logarithmic relative errors. Across both norm types, GNN maintains $\overline{\text{LRE}} < 0.5$ for all test samples. The two implementations of Hager–Higham show a constructive profile, while the version deployed in SciPy, though obtaining a slightly smaller LRE_{max} , achieves longer runtime and higher $\overline{\text{LRE}}$, which is also observed in Table 3—that empirical results of Scheme 2.

For Scheme 2, the task focuses on $\hat{\kappa}(\mathbf{A}) = 10^{\tilde{g}(\mathbf{A}; \theta)}$, the task becomes a straightforward precision where $\tilde{g}(\mathbf{A}; \theta) \approx \log_{10} (|\mathbf{A}|, |\mathbf{A}^{-1}|)$. The corresponding runtime and accuracy are reported in Table 3. Similar to the results for the 1-norm condition number in Scheme 1, GNN again achieves the best runtime performance. For 1-norm and 2-norm condition number prediction, GNN attains $\overline{\text{LRE}} < 0.5$ for all test samples, which is slightly better than the Hager–Higham method. For 2-norm condition number prediction, GNN achieves $\overline{\text{LRE}} < 0.5$ for 100% of the test samples, whereas the Golub–Kahan method achieves this threshold for only 56% of samples with 20 iterations and 67% with 60 iterations. All competing methods maintain $\overline{\text{LRE}} < 1$ across all test samples.

Comparing the empirical results of Scheme 1 and Scheme 2, GNN exhibits a relatively smaller LRE in Scheme 1 for both 1-and 2-norm cases. However, the 2-norm of a matrix is also a tricky task for estimating so the Scheme 2 is more practical for 2-norm condition number estimation. Across the tests, the dominant bottleneck in GNN approach is its inference time. In both prediction schemes, Hager–Higham (SciPy) exhibits close runtime compared to the exact method and a higher runtime than the Hager–Higham method. The favorable speed of the exact method is largely attributable to the fact that both the Exact and Hager–Higham approaches are deployed on the GPU, while Hager–Higham (SciPy) is deployed on the CPU). Besides, it is observed that Golub–Kahan method with increasing iterations achieves significant increase of runtime, though the error prone is decreased.

Table 2: Performance comparison of $g(\mathbf{A}) \approx \|\mathbf{A}^{-1}\|$ for 1-norm and 2-norm computation. Time is reported in milliseconds (ms). Logarithmic relative error (LRE) is reported in percentage (%).

Norm	Method	Mean Time (ms)	Logarithmic Relative Error (%)		Accuracy (%)	
			$\overline{\text{LRE}}$	LRE_{\max}	$\overline{\text{LRE}} < 0.5$	$\overline{\text{LRE}} < 1$
1-norm	Exact	62.27	0.00	0.00	100	100
	GNN (resp. inference)	7.57 (4.31)	1.71	7.26	100	100
	Hager–Higham	28.74	16.23	100.81	82	99
	Hager–Higham (SciPy)	59.48	18.25	94.73	82	100
2-norm	Exact	360.40	0.00	0.00	100	100
	GNN (resp. inference)	18.20 (4.39)	1.24	5.61	100	100
	Golub–Kahan (iter=20)	38.72	46.31	80.14	56	100
	Golub–Kahan (iter=60)	256.51	34.60	75.22	67	100

Table 3: Performance comparison of $g(\mathbf{A}) \approx \kappa(\mathbf{A})$ for 1-norm and 2-norm computation (updated dataset). Time is reported in milliseconds (ms). Relative error is shown in percentage (%).

Norm	Method	Mean Time (ms)	Logarithmic Relative Error (%)		Accuracy (%)	
			$\overline{\text{LRE}}$	LRE_{\max}	$\overline{\text{LRE}} < 0.5$	$\overline{\text{LRE}} < 1$
1-norm	Exact	64.93	0.00	0.00	100	100
	GNN (resp. inference)	7.35 (4.31)	2.44	12.62	100	100
	Hager–Higham	30.16	16.23	100.81	82	99
	Hager–Higham (SciPy)	57.85	18.25	94.73	82	100
2-norm	Exact	361.03	0.00	0.00	100	100
	GNN (resp. inference)	6.93 (4.26)	7.46	29.01	100	100
	Golub–Kahan (iter=20)	37.02	46.31	80.14	56	100
	Golub–Kahan (iter=60)	248.59	34.60	75.22	67	100

The Figure 3 completes the analysis of runtime and accuracy. The boxplots of LRE in Figure 3 show that the interquartile range of GNN is larger than the Hager–Higham while shorter than Hager–Higham (SciPy) for 1-norm condition estimation, though Hager–Higham and Hager–Higham (SciPy) exhibit more outliers (for failing cases); and Golub–Kahan methods (with iterations of 20 and 60) show a wide interquartile range compared to the GNN approach for 2-norm condition number estimation. In general, the outliers of the LRE scores from GNN are closer to the center than those from the Hager–Higham method for Scheme 1. Besides, we found that the GNN in Scheme 2 has a wider interquartile range and more outliers than in Scheme 1, potentially due to the increasing complexity of the tasks. In general, our GNN approach results are slightly more dispersed than Hager–Higham for 1-norm estimating and less error-prone than Golub–Kahan methods for 2-norm condition number estimating, while maintaining a significantly faster speed.

5 Limitations

Our approach relies on the quality of the training data: the closer the distributions of the training and test sets, the better the accuracy of the model. Ideally, the test data is expected to follow a distribution similar to that used to train the model; however, this is not strictly required, as we have not yet evaluated the model’s generalization ability outside this scenario. Future studies will investigate which factors (e.g., matrix sizes or matrix element magnitude) are most sensitive and contribute to performance loss on testing data. In this paper, we focus on the formulation of our approach and demonstrate the capabilities of GNNs for condition number estimation. We have not optimized the model architecture, hyperparameters, or training routine, so readers may achieve further refined results by tuning these settings. Besides, as observed in the experiments, the dominant runtime for condition number prediction for GNN lies in the inference. Therefore, potential speedup can be achieved with ONNX [3].

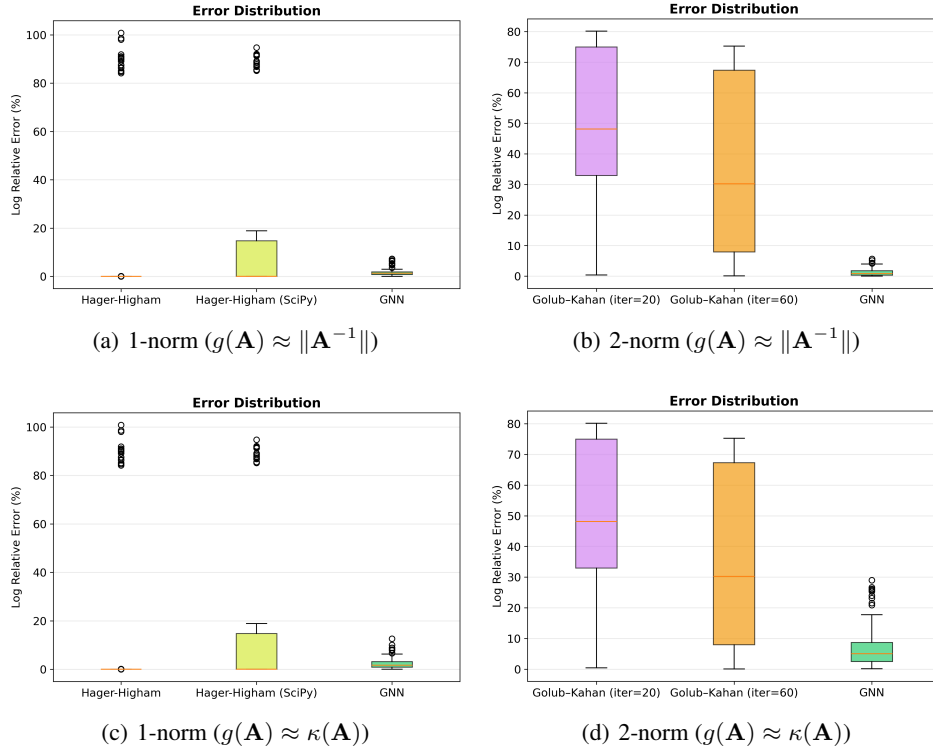


Figure 3: Boxplot of the error.

6 Conclusion

We proposed a rapid condition number estimation approach using graph neural networks for sparse linear systems. We propose two prediction schemes, one by decomposing the condition number into an exactly computable forward norm and a neural-network-predicted inverse norm, and another by directly predicting the matrix condition number. Extensive experiments for the two schemes show that, with a limited amount of data, our method achieves orders of magnitude speedup over exact computation and compares favorably against the Hager–Higham and Golub–Kahan methods at a certain scale in terms of speed while maintaining competitive accuracy. The architecture combines graph convolutional layers to capture sparsity patterns with global feature encoders for statistical properties, enabling effective generalization. Future work will explore optimized GNN architectures and end-to-end feature engineering.

We believe that our work can be beneficial to existing work on precision tuning (e.g. [1]), since precision usage is highly dependent on condition number and a faster estimation of it can significantly boost the applications.

References

- [1] E. Carson and X. Chen. Precision autotuning for linear solvers via reinforcement learning, 2026.
- [2] A. K. Cline, C. B. Moler, G. W. Stewart, and J. H. Wilkinson. An estimate for the condition number of a matrix. *SIAM Journal on Numerical Analysis*, 16(2):368–375, 1979.
- [3] O. R. developers. Onnx runtime. <https://onnxruntime.ai/>, 2021.
- [4] G. H. Golub and C. F. Van Loan. *Matrix Computations*. Johns Hopkins University Press, Baltimore, MD, 4th edition, 2013.
- [5] W. W. Hager. Condition estimates. *SIAM Journal on Scientific and Statistical Computing*, 5(2):311–316, 1984.
- [6] N. J. Higham. A survey of condition number estimation for triangular matrices. *SIAM Review*, 29(4):575–596, 1987.
- [7] N. J. Higham. Estimating the matrix condition number. *SIAM Journal on Scientific and Statistical Computing*, 9(2):273–287, 1988.

- [8] N. J. Higham. FORTRAN codes for estimating the one-norm of a real or complex matrix, with applications to condition estimation. *ACM Transactions on Mathematical Software*, 14(4):381–396, 1988.
- [9] N. J. Higham. Algorithm 674: Fortran codes for estimating the one-norm of a real or complex matrix, with applications to condition estimation. *ACM Trans. Math. Softw.*, 15(2):168, June 1989.
- [10] D. P. Kingma and J. Ba. Adam: A method for stochastic optimization. In *International Conference on Learning Representations*, 2015.
- [11] T. N. Kipf and M. Welling. Semi-supervised classification with graph convolutional networks. In *International Conference on Learning Representations*, 2017.
- [12] A. Paszke, S. Gross, F. Massa, A. Lerer, J. Bradbury, G. Chanan, T. Killeen, Z. Lin, N. Gimelshein, L. Antiga, et al. PyTorch: An imperative style, high-performance deep learning library. In *Advances in Neural Information Processing Systems*, volume 32, pages 8024–8035, 2019.
- [13] N. Srivastava, G. Hinton, A. Krizhevsky, I. Sutskever, and R. Salakhutdinov. Dropout: A simple way to prevent neural networks from overfitting. *Journal of Machine Learning Research*, 15(56):1929–1958, 2014.
- [14] L. N. Trefethen and I. Bau, David. *Numerical Linear Algebra*. SIAM, Philadelphia, PA, 1997.
- [15] S. Xu and J. Zhang. *Matrix Condition Number Prediction with SVM Regression and Feature Selection*, pages 491–495.

A Loss during training

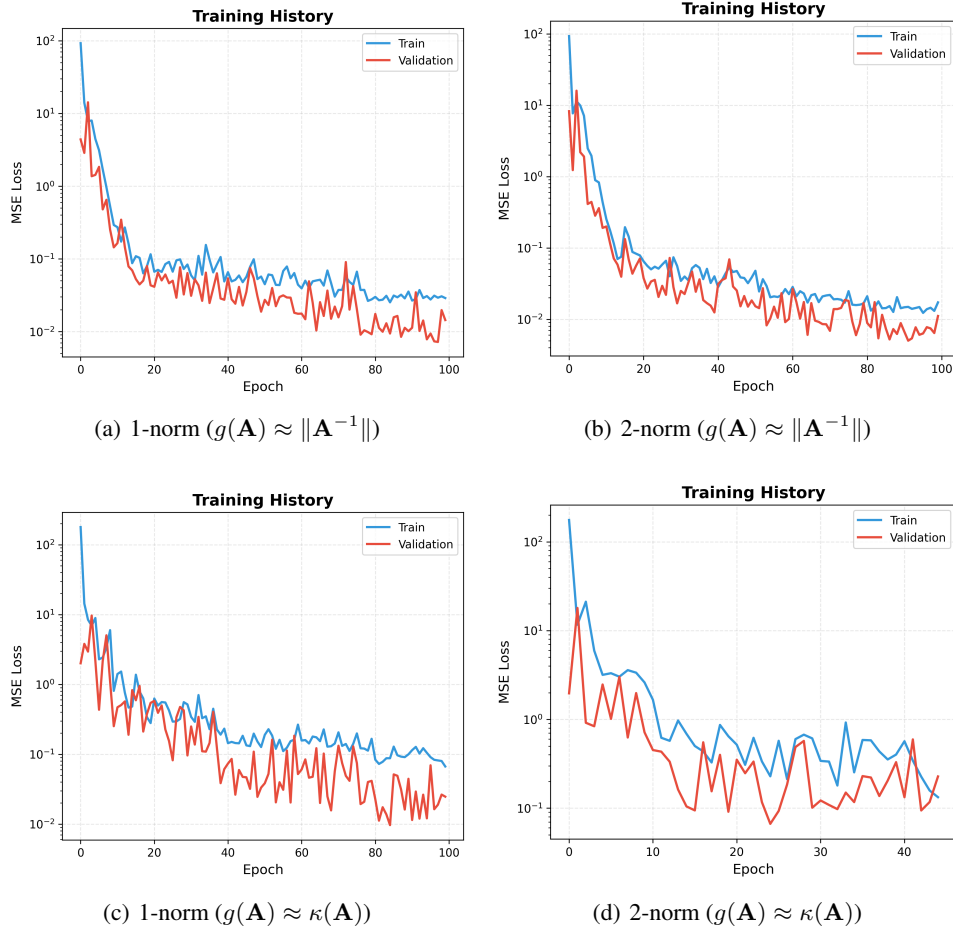


Figure 4: Loss during training.